The Influence of the Boundary Layer State and Reynolds Number on Film Cooling and Heat Transfer on a Cooled Nozzle Guide Vane

Hans Reiss, Albin Bölcs
Laboratoire de Thermique Appliquée et de Turbomachines (LTT)
Swiss Federal Institute of Technology
CH-1015 Lausanne, Switzerland

ABSTRACT
Film cooling and heat transfer measurements were carried out on a cooled nozzle guide vane in a linear cascade, using a transient liquid crystal technique. Three flow conditions were realized : the nominal operating condition of the vane with an exit Reynolds number of 1.47e6, as well as two lower flow conditions: Re_{2L}=1.0e6 and 7.5e5. The vane model was equipped with a single row of inclined round film cooling holes with compound angle orientation on the suction side. Blowing ratios ranging form 0.3 to 1.5 were covered, all using foreign gas injection (CO_2) yielding an engine-representative density ratio of 1.6. Two distinct states of the incoming boundary layer onto the injection station were compared, an undisturbed laminar boundary layer as it forms naturally on the suction side, and a fully turbulent boundary layer which was triggered with a trip wire upstream of injection.
The aerodynamic flow field is characterized in terms of profile Mach number distribution, and the associated heat transfer coefficients around the uncooled airfoil are presented. Both detailed and spanwise averaged results of film cooling effectiveness and heat transfer coefficients are shown on the suction side, which indicate considerable influence of the state of the incoming boundary layer on the performance of a film cooling row. The influence of the mainstream flow condition on the film cooling behavior at constant blowing ratio is discussed for three chosen injection regimes.

NOMENCLATURE

A_b,A_h	[m^2]	hole base area, hole exit area
d	[mm]	cooling hole diameter
DR	[1]	coolant-to-gas density ratio ρ_c/ρ_g
G_{CO2}	[1]	blowing ratio $u_c\rho_c/u_g\rho_g$ using CO_2
l_h	[m]	cooling hole length
L	[m]	real chord of airfoil
L_x	[m]	longitudinal integral lengthscale
M	[1]	isentropic Mach number $u/(\kappa RT)^{0.5}$
p	[Pa]	pressure; spanwise hole spacing (pitch)
q	[W/m^2]	heat flux density
R	[J/kg/K]	ideal gas constant
Re_{2L}	[1]	cascade exit Reynolds number $(u_2L)/\nu$
R_a,R_z,R_t	[µm]	surface roughness parameters (DIN4768)
s	[m]	surface distance from profile leading edge
s*	[m]	surface distance from injection location
T	[K]	temperature
Tu	[%]	turbulence intensity
u	[m/s]	flow velocity

GREEK

α	[$W/(m^2K)$]	local heat transfer coefficient
β	[°]	spanwise inclination angle
γ	[°]	compound angle
η	[1]	film cooling effectiveness
φ	[°]	streamwise inclination angle
ρ	[kg/m^3]	density
ν	[m^2/s]	kinematic viscosity

SUBSCRIPTS

aw	adiabatic wall
c	coolant
f	with film cooling
g	main flow gas
r	recovery conditions
t	total conditions
injection	main flow conditions at injection location

INTRODUCTION
Heat transfer plays a important role in the development of modern gas turbines. Especially the design of strongly cooled first stages of a turbine requires detailed knowledge of heat transfer and film cooling effectiveness is needed, and typically empirical correlations as well experimental data on film cooling available in the literature are employed. However, the applicability of the published data remains in many cases questionable. For example, numerous experimental studies use flat plate or blunt-body models to investigate the cooling performance of isolated injection stations. On a strongly cooled airfoil with multiple cooling rows, however, the cooling performance of an individual row may be altered considerably, since the presence of upstream cooling rows is likely to change the state of the boundary layer with respect to a single-station experiment. The boundary layer is transitional or fully turbulent rather than laminar as it is the case in many single-station experiments. As has been shown before by Drost and Bölcs (1999) the film cooling effectiveness is strongly influenced by the nature of the incoming boundary layer. Nirmalan and Hylton (1990) performed heat transfer experiments on a first-vane model equipped with downstream film cooling, with and without leading edge cooling over a wide range of main flow and injection conditions. They reported that high leading edge blowing can actually increase heat transfer over the entire pressure side and associated this to increased turbulence levels caused by the leading edge injection. This

Submitted for the
45th ASME Gas Turbine and Aeroengine Technical Congress, Exposition and Users Symposium
8-11 May 2000, Munich, Germany

confirms that the state of the incoming boundary layer onto a downstream film row has an effect on its cooling performance. The fact that they found very little effect on the suction side might be associated with the strong main flow acceleration around the leading edge towards the suction side and therefore smaller influence of the upstream injection due to partly re-laminarization. These studies show that the use of single-station data may be mis-estimating by far the actual heat transfer in a real-engine situation.

The influence of the main flow conditions on film cooling has been reported contradictorily in the literature. Mehendale and Han (1993) reported a slight increase of film cooling effectiveness for higher main stream Reynolds numbers for a showerhead cooling experiments. Reiss and Bölcs (2000) reported decreased effectiveness values for increased free stream Mach and Reynolds numbers. Wadia and Nealy (1985) carried out cylinder experiments and detected slightly higher effectiveness when increasing the Reynolds number, while the Mach number was held constant. In the same study, they report decreasing effectiveness with Mach number, when the Reynolds number is held constant.

The objective of the work presented in this paper is to address both issues mentioned above: what is the effect of the state of the incoming BL on an isolated film cooling row, and which role play the main flow parameters exit Mach and Reynolds number on film cooling at maintained injection rates. This was set in practice by investigating a single row injection station on the suction side of a turbine airfoil in a linear cascade at various free stream flow conditions and injection rates, and with laminar and fully turbulent incoming boundary layer at injection location. In the following sections the a description of the data reduction technique and experimental apparatus are given, followed by the presentation of the obtained experimental results and discussion.

DATA ANALYSIS

The local convective heat flux into a film-cooled surface can be written as

$$q = \alpha_f (T_{aw} - T_w) \tag{1}$$

where the driving temperature difference for the definition of α_f is the adiabatic wall temperature T_{aw} (which is the effective gas temperature at the wall) minus the surface temperature of the model. T_{aw} is unknown and depends on the temperatures of the main stream and the injected coolant gas, and on the mixing between jets and main flow. It can be written in dimensionless form as the film cooling effectiveness

$$\eta = \frac{T_{aw} - T_{rg}}{T_{tc} - T_{tg}} . \tag{2}$$

Other definitions for the film cooling effectiveness are also known in the literature, often referring entirely to recovery temperatures in both nominator and denominator. For this study, the denominator contains coolant and mainstream total temperatures. By using this definition both parameters α_f and η are independent of the temperature boundary conditions. They are thus a function of the aerodynamic flow field alone, as long as constant gas properties are supposed Vedula and Metzger (1991).

The present measurements were carried out with the transient liquid crystal technique, which consists of exposing a pre-conditioned model rapidly to an established flow field at a different temperature for a limited amount of time. The duration of an experiment is chosen such that the penetration of the heat pulse is small compared the model wall thickness. By considering one-dimensional transient heat conduction into a semi-infinite solid, together with convective boundary condition, an analytical model for the surface temperature evolution can be established (Drost and Bölcs (1996)). For the temperature levels used in this study, the heat flux due to radiation can be neglected compared to the convective heat flux. The local wall temperature rise during an experiment is monitored by detecting the appearance of a certain color of the liquid crystal coating with video cameras and an image processing computer.

A multiple tests regression scheme is used to determine the two unknowns α_f and η: Several tests (typically 6-8) are performed at identical free stream conditions and blowing ratio, but varied coolant injection temperature. The model initial temperature for each test is adjusted in a range of –25° to 5°C to compensate for the time variation of the liquid crystal color play caused by the different coolant temperatures. Doing so the duration between model insertion and liquid crystal event in was kept in range of 2 to 5 seconds for which the semi-infinite assumption is valid, and the uncertainty on the time detection of the liquid crystal events is still acceptable (an inevitable effect due to model insertion and the time resolution of the image processing system). A least-square regression analysis over the ensemble of tests allows to yields α_f and η. An inconvenience of this multi-regression approach is that the variation of injection temperature over a range of 30 K causes - at constant blowing ratio - slight changes of the density ratio, and thus momentum ratio of the order of 8% over an ensemble of tests results.

Measurement uncertainties were computed according to Kline and McClintock (1953) using the governing least-square equation for an ensemble of tests, and introducing the existing uncertainties for temperatures, thermal properties and measurement time. Before it was verified that the ensemble is in statistical equilibrium, i.e. it contains a sufficiently large number of individual tests so that the relative deviations in α_f and η were small (below 1%) when the test number was further increased. The resulting uncertainty for the heat transfer coefficient is about 6%, and for the film cooling effectiveness 4% (for η=0.3) to 10% (for η=0.1). For more details on the measurement technique and the data analysis see Reiss et al. (1998) or Hoffs et al. (1995).

TEST FACILITY AND INSTRUMENTATION

Linear Cascade Test Facility

Fig. 1 shows the wind tunnel holding the linear cascade test section with 5 blades. The flow channel is 99mm wide, and the blade pitch is fixed to 64mm. Straight or contoured endwalls were used, and resulting flow field is essentially 2-dimensional. Two tailboards and bypass vanes are installed for adjustment of flow conditions, and in particular to achieve good flow periodicity over the two center passages of the cascade. Up to 10 kg/s air can be supplied continuously to the test stand at pressure levels of up to 2.5 bar, allowing operation of the cascade at sub- and transonic flow conditions. Maximum exit Reynolds numbers of 1.7e6 (based on a chord length) can be achieved. The free stream turbulence level of 10% is obtained by a square bar-type turbulence grid inserted upstream of the test section.

The airfoil for heat transfer measurements is situated in the center of the cascade. It can be removed from the flow for preconditioning prior to the transient experiment, and replaced by an aerodynamic dummy blade.

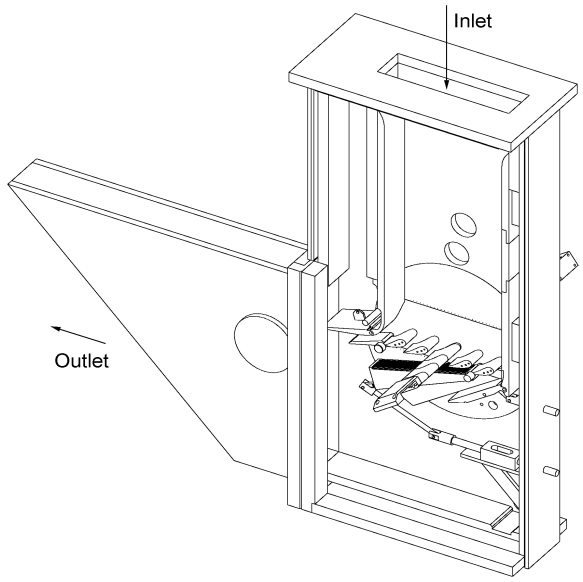

Fig. 1 – Wind Tunnel with Linear Cascade

The insertion mechanism is shown in Fig. 2 (preconditioning position on the left, measurement position on the right). The mechanism is activated via a computer-controlled pneumatic cylinder. The insertion time is less than 0.1s, which is a good approximation of a step change of the temperature boundary condition that is supposed for the data analysis. The unsteady effect of the model insertion on the flow field in the channel center are considered negligible in view of the test duration of about 5 seconds.

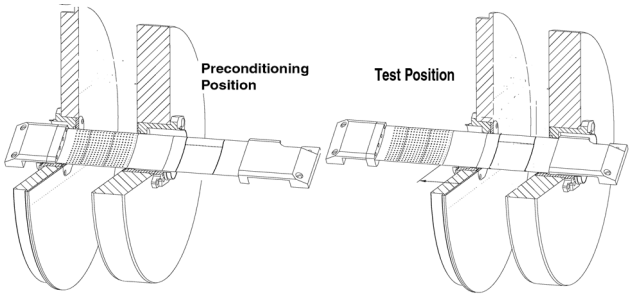

Fig. 2 – Rapid Insertion Mechanism for Blade Model

The center blade slides in a tightly fit Teflon guidance on the 'dummy' side in order to avoid misalignment of the blade with the neighboring blades, and to prevent bending of the center blade by the aerodynamic forces. Pneumatic seals close tightly around the blade and additional guidance and centering. One sidewall (disk on the right in Fig. 2) carries several small optical access windows for the video cameras.

For further flow characterization, one of the sidewalls can be replaced by an optical access window for laser-2-focus measurements of the flow vectors in the passages.

Coolant Gas Supply

The coolant gas is provided from a large reservoir with a choked orifice. This allows accurate adjustment of the flow rate by setting the total pressure in the reservoir and the orifice diameter. The coolant flow is switched on just before insertion of the model by a mechanical valve which is actuated when pulling the blade into the wind tunnel. During the transient tests, the flow rate is accurately monitored with laminar flow elements. The coolant injection temperature is pre-set with electrical heaters. In order to reduce internal heat losses, all supply tubes are purged with air flow prior to an experiments. The measurement system is such that the blowing ratio is constantly controlled and adjusted, in order to account for small variations in main flow conditions that may occur during a measurement campaign.

Instrumentation

A removable total pressure probe is located upstream of the test section; it is completely retrieved from the channel before an actual heat transfer experiment to avoid the influence caused by the wake of the probe. The total temperature is taken with a total temperature probe in the upstream settling chamber. The test section itself (shown in Fig. 3) is equipped with a series of static pressure taps in the side walls both up- and downstream of the cascade.

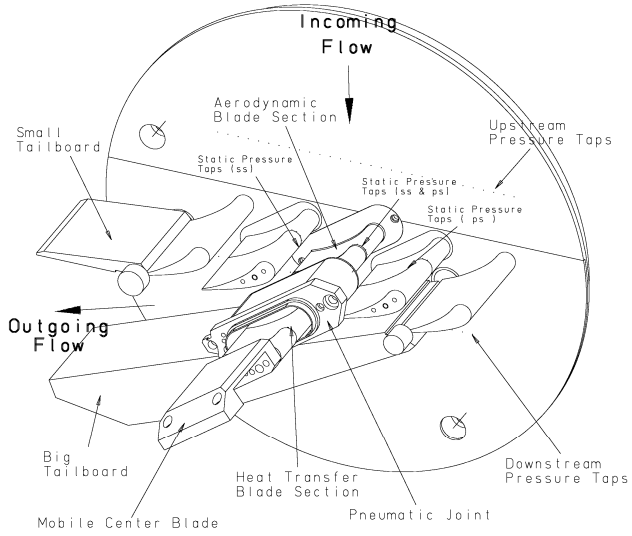

Fig. 3 – Linear Cascade Test Section

Static pressure taps are distributed around the center and the two adjacent blades at mid-span. By comparing static pressure profiles of pressure- or suction side on the center blade with the pressure- or suction side on the respective neighboring blade, the periodicity of the flow can be verified. The center blade is assembled from an 'aero' section (see on the left of Fig. 4) carrying the pressure taps and a machined-on reference grid used for the image processing system. Traversing the center blade in small increments through the channel permits determination of the detailed pressure distribution on the entire model surface.

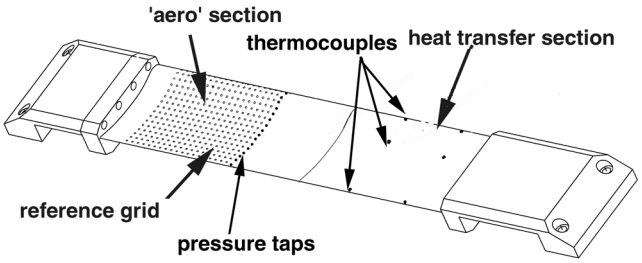

Fig. 4 – Center Blade with Instrumentation

The exchangeable 'heat transfer' section of the center blade is shown on the right of Fig. 4. It consists of machined Perspex™ and carries the film cooling holes, as well as embedded thermocouples for the determination of the initial temperature distribution of the preconditioned model. A single plenum chamber feeds all cooling

holes; it also holds a total pressure and a fast-response total temperature probe for the acquisition of transient coolant gas conditions. The model surface is coated with commercial narrow-band encapsulated thermochromic liquid crystals (color play over a temperature range of 30-31°C, Hallcrest™, U.K.) with black backing. The crystals are polished to obtain a smooth surface with good repeatability. Typically, a surface roughness of R_z=9±1.5 µm, R_a=2.4±0.5µm, and R_t=15±2.7µm is achieved.

Aerodynamic Flow Conditions

The operating conditions for the current study are characterized by surface distributions of isentropic Mach numbers around the center blade, Fig. 5. The highest Reynolds number case (Re_{2L}=1.47e6, M_2=0.85) represents the nominal operating conditions of the vane profile. The flow is first further accelerated after injection, with a peak Mach number of 0.96, and then decelerated towards the trailing end of the suction side. The two lower flow conditions (Re_{2L}=1.0e6, M_2=0.60, and Re_{2L}=0.75e6, M_2=0.41) have an almost homogeneous Mach number distribution after injection, with a slight decrease towards the trailing edge. The main flow Mach number values at actual injection location, which were subsequently used to compute the blowing ratio, are marked to Fig. 5. The good flow periodicity can be seen in the passage flow field, gathered with a laser-2-focus system at about 70 measurement points in the midspan plane for nominal operating conditions.

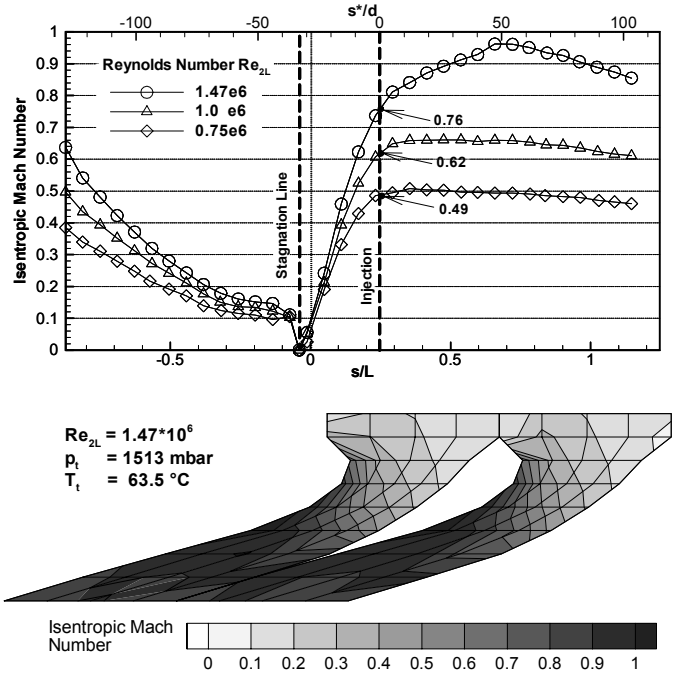

Fig. 5 – Flow Characterization for the Linear Cascade : Profile Mach Number and Passage Flow Field

FILM COOLING CONFIGURATION

The airfoil carries a single row of oriented film cooling holes with a diameter 0.87% of axial chord. Its position with respect to the airfoil profile can be seen in Fig. 6. Table 1 lists the geometric parameters in terms of orientation, hole length, spacing and surface area ratio according to the definitions given in Fig. 7.

p/d	s/L	φ	β	γ	l_h/d	A_h /A_b
3.6	0.25	40°	45°	50°	7.3	1.6

Table 1 – Details of Single Row Injection Configuration

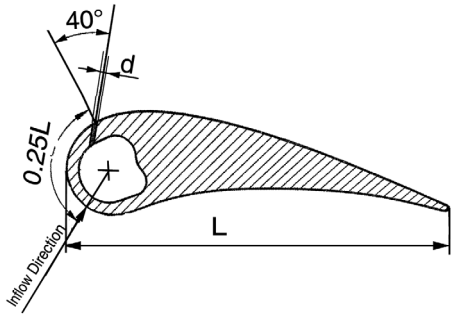

Fig. 6 – Airfoil Profile with Film Cooling Injection on Suction Surface

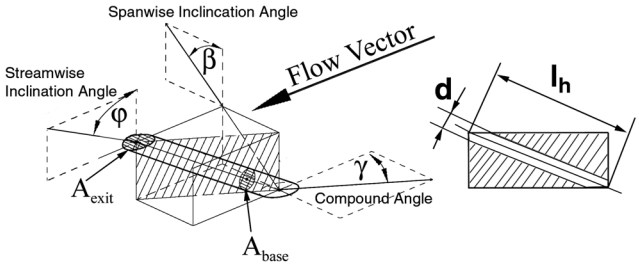

Fig. 7 – Definition of Injection Geometry

For the bulk of measurements in this study the incoming boundary layer for the cooling row was triggered with a fine trip wire which was pasted onto the surface at a surface position of s/L≈0.17 (see Fig. 8). This proved to be sufficiently far from the highly accelerated zone around leading edge that no re-laminarization occurred. Immediate laminar-turbulent transition was found with very short transition length was found in preliminary tests.

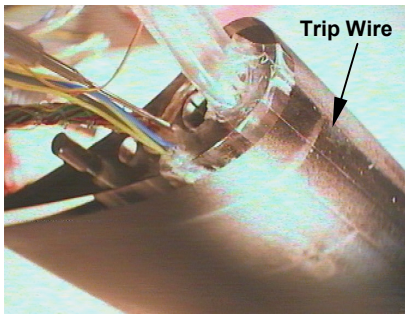

Fig. 8 – Triggering of Boundary Layer Transition with Trip Wire

TEST CONDITIONS FOR FILM COOLING EXPERIMENTS

The test matrix for this study as given in Table 2 was defined with two objectives : firstly, allow a comparison of laminar and turbulent incoming boundary layer at various blowing conditions, and secondly, compare several main stream conditions at constant blowing ratios. For the latter comparison, it was chosen to investigate different distinct injection regimes (weak blowing with good coverage in hole vicinity, intermediate blowing, and high blowing with the tendency of jet lift-off).

Main Flow	$\mathbf{Re_{2L}}$	$1.47 \cdot 10^6$	$1.00 \cdot 10^6$	$7.50 \cdot 10^5$
	$\mathbf{M_2}$	0.85	0.60	0.41
	$\mathbf{p_t}$ [mbar]	1513	1275	1175
	$\mathbf{T_t}$ [°C]	63	61	60
Coolant Flow	$\mathbf{M_{injection}}$	0.76	0.62	0.49
	$\mathbf{G_{CO2}}$	0.3 0.7 1.0 1.3 1.5	0.3 1.0 1.5	0.3 1.0 1.5
Boundary Layer State		turbulent laminar	turbulent	turbulent

Table 2 – Test Conditions

RESULTS AND DISCUSSION

Baseline Heat Transfer

Spanwise averaged results of heat transfer coefficients on a solid airfoil (without film cooling injection) are shown in Fig. 9. The curves of laminar BL are staggered in terms of Reynolds number. Peak values occur near the blade leading edge, but are slightly shifted towards the suction side with respect to the location of the actual stagnation line of the flow. BL transition occurs at the same location for all three flow conditions. For the highest flow condition, Re_{2L}=1.47e6, the heat transfer coefficients with the trip wire in place are shown as well. It illustrates clearly the fully turbulent BL over the entire suction surface, with very high values of heat transfer coefficient at injection location.

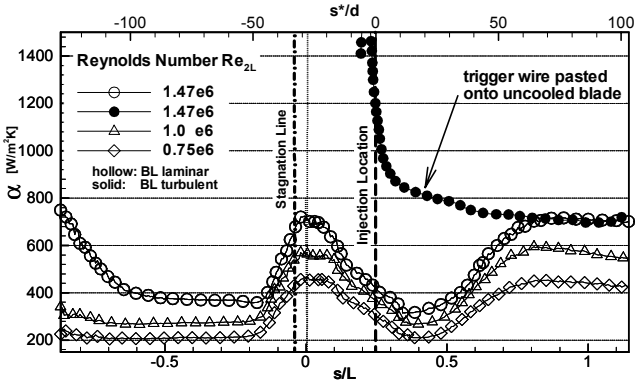

Fig. 9 – Uncooled Blade : Spanwise Averaged Heat Transfer Coefficient Results

Detailed Heat Transfer Coefficient Results

Detailed distributions of local heat transfer coefficients are shown on top of Fig. 10. The spatial resolution of the detailed results is approximately 20 data points per hole diameter, with exception of the cases at low Reynolds number and blowing ratios G=1.0 and 1.5 (on the very right, line 3 and 5). For these two cases only few valid data points could be gathered upstream of and around the holes (see zones with distinct patches of parallel contours).

The plots show a zoomed region around the cooling holes and are arranged according to the test matrix in Table 2: the blowing ratio is varied from top to bottom, and the main flow condition from left to right.

The main flow direction is to the right. The first two columns contain the results for nominal cascade operating conditions with laminar (very left), and turbulent (second from left) incoming BL. The difference in boundary layer state can clearly be illustrated without injection (top row): For the laminar case, very low levels of heat transfer coefficients of about 300 W/m^2K are apparent upstream of the holes exits. The exits cause traces of increased heat transfer, which merge further downstream, i.e. the holes do locally disturb the laminar boundary layer and cause increased energy exchange to the wall. At about 20 hole diameters downstream, the lateral gradients are mixed out and the overall level of heat transfer is around 900 W/m^2K. In contrast, in the case of turbulent BL the highest heat transfer coefficients occur upstream of the holes, and it decays further downstream. The holes cause only a very weak perturbation which mixes out rather quickly. The overall level of heat transfer coefficients at 25 hole diameters downstream are comparable for both the laminar and the turbulent case.

A look at the cases with coolant injection reveals, as expected, the formation of distinct streaks with increased heat transfer coefficients of varying strength. This indicates the additional mixing that is associated with the counter-rotating vortices of the coolant jets. The associated double-streaks at both sides of the jets is most clearly seen for the weak blowing ratio of 0.3. Interestingly, at this low blowing in the presence of the turbulent BL, the film injection causes the heat transfer coefficient to decay faster than in the unblown case. This can be explained with the creation of a laminar sublayer by weak but well-attached coolant jets. At higher blowing ratios, the overall level of heat transfer coefficient is slightly increased, but stays of about the same order of magnitude, indicating that the total additional mixing caused by the jets does not excessively enhance local heat transfer. Clearly, the effect of stronger blowing changes the jet trajectories from well aligned with the main flow direction to rather curved, as a results of the compound angle orientation of the holes. As a general finding, the zones of increased heat transfer are more pronounced for the turbulent BL.

When comparing the heat transfer distributions along the lines (i.e. comparing the three different main flow conditions with each other,) one can state that heat transfer takes place on a generally much lower level, and the effect of locally decreased heat transfer due to a laminar sublayer does not occur as it did for the highest Reynolds number case. Rather the unblown case exhibits wakes of low heat transfer, which may be attributed with locally occurring re-laminarization behind the hole exits without injection. Even weak blowing enhances heat transfer, and therefore delays the decay of the general level of heat transfer. The wakes of the cooling holes are, however, more confined. At Re_{2L}=1.0e6 as the only case, heat transfer coefficient rises substantially with stronger blowing, whereas for all other flow conditions stronger blowing does not increase much further the heat transfer coefficients.

Spanwise Averaged Heat Transfer Coefficients Results

The spanwise averaged heat transfer coefficients are shown in Fig. 11 in a pseudo-3D presentation of the suction surface: The different blowing ratios tested are actually arranged along the 'span' of the airfoil, in order to give an intuitive image of the behavior of the film cooling row. Following the span from front to back means actually going from no injection towards high blowing ratios. The two graphs on the left contain the results for the nominal main flow conditions, laminar and turbulent BL, and the lower Re_{2L} cases on following to the right. Comparing the two graphs on the left hand side shows that the averaged heat transfer continues to rise slightly as the injection rate is increased at laminar incoming BL. This effect is most

pronounced in the near hole region. The turbulent case at the same Reynolds number exhibits only very weak dependence of heat transfer on the blowing, as was highlighted already with the detailed heat transfer results. The intermediate and low Reynolds number cases show a stronger dependence of heat transfer coefficient on the injection rate, which is also extended further downstream.

Detailed Effectiveness Results

The film cooling effectiveness results are shown in a similar arrangement of contour plots in Fig. 12. The coverage with coolant is considerably better for the laminar cases as compared to the turbulent ones. In contrast to the laminar case where relatively good lateral spread is detected, the jets don't interact much or merge laterally with turbulent incoming BL, instead the traces remain separated. For laminar BL, at an intermediate blowing ratio of G=1.0, very good coverage is detected in the near-hole region. Again - as described before with the heat transfer results - the jet trajectories start out aligned with the main flow at weak blowing, but gradually deviate laterally as blowing is increased.

For both the laminar and the turbulent BL state, the injection row exhibits the typical behavior that has often been reported in the literature: good coverage with only small downstream extension for weak blowing, then optimum coverage for intermediate blowing ratios, and loss of coolant due to jet lift-off at higher blowing ratios.

This typical characteristics is apparent on both laminar and turbulent BL, but on very different overall levels of effectiveness. The incoming turbulent boundary layer seems to be responsible for a substantial loss of coolant to the main flow due to much more intense mixing. The lateral spread of the jets in the laminar case is much stronger. They merge very well to create very high levels of effectiveness also between the jet trajectories, whereas in the turbulent case, the lateral spreading is very poor and the lateral extension of the traces of high effectiveness stays small. This effect may be explained by a much stronger penetration of highly turbulent main flow between the jets, and consequently by stronger dilution of coolant gas. In the laminar case, this penetration is weaker, and the tendency to dilute the coolant is much weaker, therefore allowing the jets to diffuse more laterally and create a good overall coverage.

The characteristic behavior of the cooling row (best performance for intermediate blowing ratios) was also measured at the lower main flow conditions, most clearly for the lowest Reynolds number case Re_{2L}=0.75e6.

Spanwise Averaged Effectiveness Results

Fig. 13 gives laterally averaged effectiveness distributions are presented similarly to the corresponding heat transfer results, in the form of pseudo-3D graphs. The above described effect of loss of coolant due to an incoming turbulent BL is clearly noticeable. A zone of high effectiveness is developing for high blowing a little downstream of injection location. A comparison between the three main flow conditions reveals that far downstream the effectiveness behaves very similar for all Reynolds numbers, but in the immediate and extended near hole region the characteristics are very different. At lowest Reynolds number Re_{2L}=0.75e6, a dark zone of elevated η in direct proximity of the injection location is developing as the blowing is increased, and it slightly diminishes again towards the highest blowing conditions. For the intermediate Reynolds number Re_{2L}=1.0e6 the same dark zone of elevated η appears, but disappears almost completely for the high blowing ratios. However, further downstream a new zone of good coverage appears. This is typical for jet lift-off and re-attachment for high blowing ratios. At the highest Reynolds number Re_{2L}=1.47e6 the distinct zone of high η at low injection is completely missing, but at higher blowing ratios a zone of relatively elevated values occurs. It is located downstream of injection, but not as far as the re-attachment zone described above for Re_{2L}=1.0e6. The data shows that the qualitative behavior of an injection row – for a given blowing ratio - may actually be changed by the main flow regime. In this study, this change consisted of a combined change of Reynolds- and Mach number.

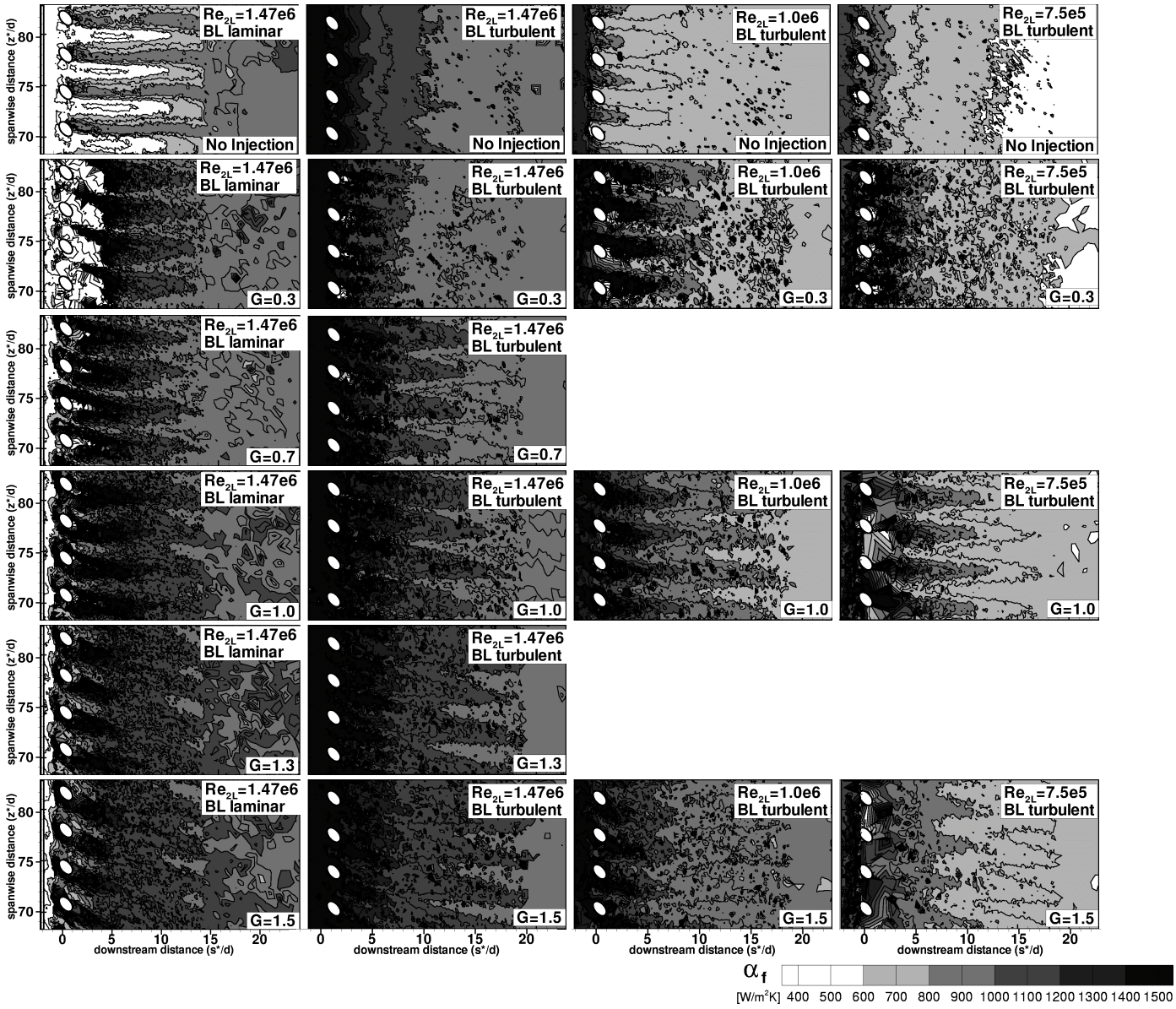

Fig. 10 - Detailed Heat Transfer Coefficient Distributions

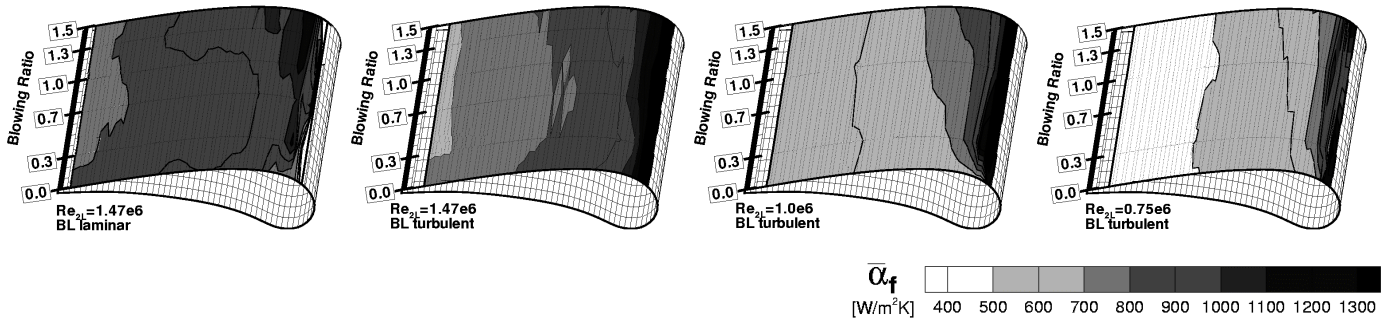

Fig. 11 – Spanwise Averaged Heat Transfer Coefficients

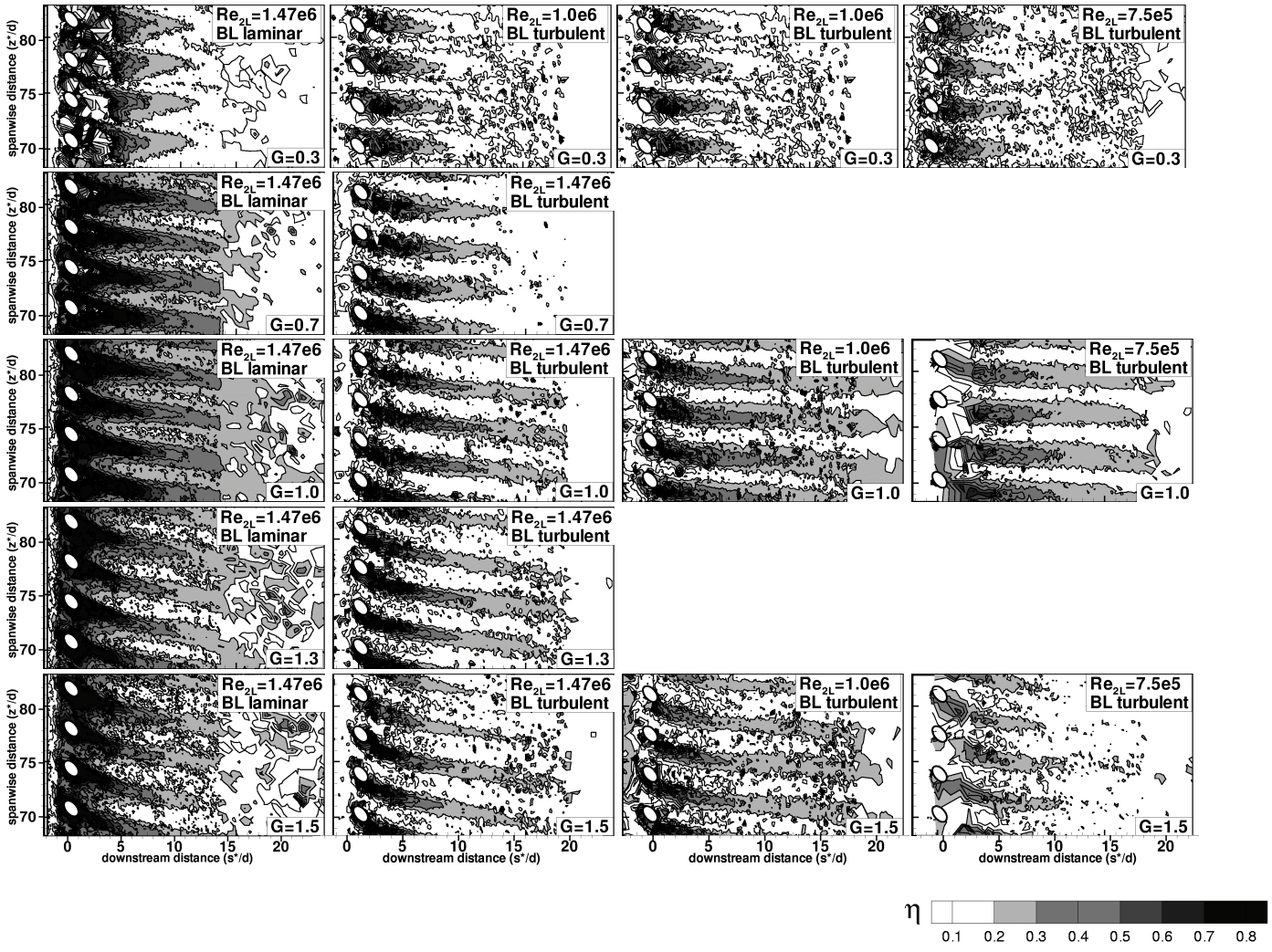

Fig. 12 - Detailed Film Cooling Effectiveness Distributions

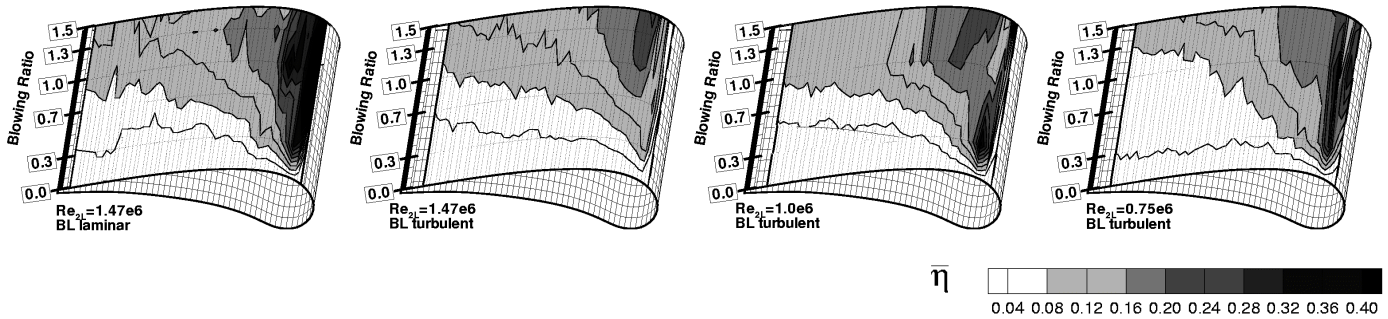

Fig. 13 – Spanwise Averaged Film Cooling Effectiveness

Effect of the Incoming Boundary Layer State

A more quantitative discussion is undertaken with Fig. 14, which shows averaged effectiveness as a function of blowing ratio, for four chosen surface positions: 10, 20, 40 and 80 hole diameters from injection. The hollow symbols denote the laminar BL case. The qualitative behavior is comparable at all surface locations, but effectiveness values of the laminar cases are generally higher at intermediate blowing ratios, with exception of the surface location 20d, where values are similar (round symbols). The biggest difference between laminar/turbulent BL is visible at 10d, in immediate proximity of injection, where η is up to 50% higher for the laminar case.

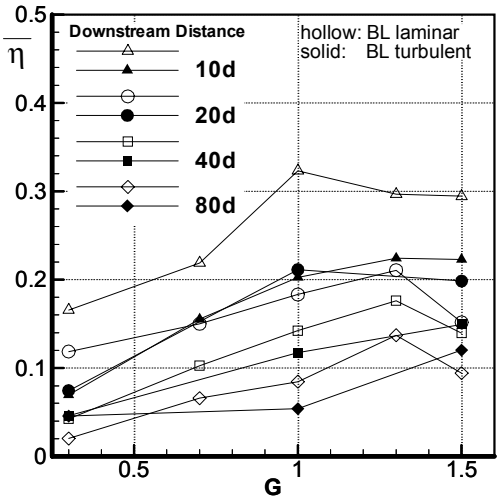

Fig. 14 – Influence of BL State on Spanwise Averaged Effectiveness

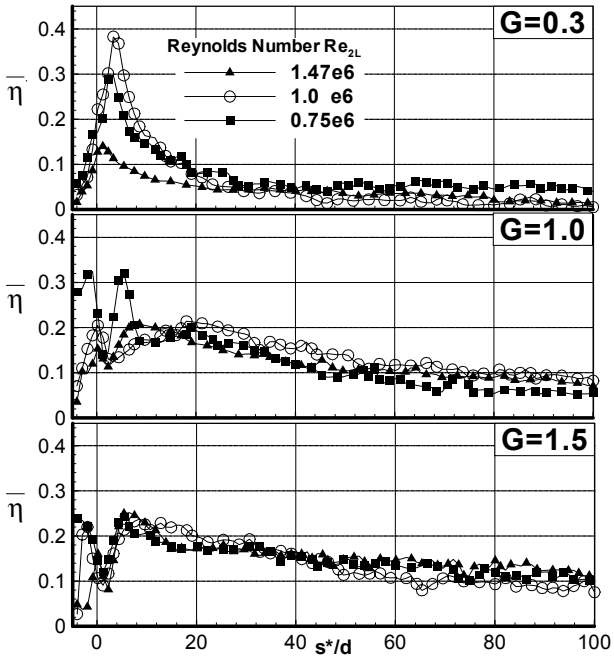

Fig. 15 – Influence of Reynolds Number on Spanwise Averaged Effectiveness

Effect of the Main Flow Conditions

Influence of the main flow conditions is addressed in Fig. 15, which shows curves of spanwise averaged effectiveness for all three Reynolds number/Mach number combinations – at the injection regimes low (on top), intermediate (in the middle) and intense blowing (bottom). At low blowing ratio G=0.3, the best effectiveness in the near hole region was measured for Re_{2L}=1.0e6, whereas at about 40 hole diameter downstream, all three Reynolds number have similar values. Far downstream, the staggering is inverted, and the best η is achieved at lowest the Reynolds number.

For intermediate blowing G=1.0, highest effectiveness was measured for Re_{2L}=0.75e6 in the near-hole region; far downstream, and the two other Reynolds number show higher effectiveness values. For G=1.5, the differences in η are very small, which makes a detailed quantitative discussion difficult.

CONCLUSIONS

Detailed experimental data from heat transfer and film cooling measurements on a nozzle guide vane were presented showing the influence of the incoming boundary layer state on the injection station, as well as the effect of main flow conditions at constant blowing ratio.

It was shown that an incoming turbulent BL decreases considerably the obtained effectiveness values, which is an important finding in terms of validity of experimental data gathered on single injection stations with a laminar BL for actual engine conditions.

It was also shown that a change of main flow conditions (in this study a combined change of Reynolds and Mach number) - at constant blowing ratio – can have adverse effects on the film effectiveness and heat transfer even on the same airfoil model during the same experiment. Higher Mach and Reynolds number may increase or decrease the film cooling effectiveness, depending on the surface location and the intensity of injection. No uniform trend could be established that would be generally applicable for the entire model surface and all injection conditions.

REFERENCES

Drost, U. and Bölcs, A., 1996: The Transient Liquid Crystal Technique Applied for the Investigation of Flat Plat and Showerhead Film Cooling. *Measurement Techniques, Zürich, Vol.97-GT-26*

Drost, U. and Bölcs, A., 1999: Investigation of Detailed Film Cooling Effectiveness and Heat Transfer Distributions on a Gas Turbine Airfoil. *ASME Journal of Turbomachinery, Vol.121, April 1999, pp 233-242*

Hoffs, A., Bölcs, A. and Harasgama, P., 1995: Transient heat transfer experiments in a linear cascade via an insertion mechanism using the liquid crystal technique. *Journal of Turbomachinery, Vol.119, Jan. 1997, pp 9-13*

Kline, S.J. and McClintock, F.A., 1953: Describing Uncertainties in Single-Sample Experiments. *Mechanical Engineering, January 1953*

Mehendale, A.B. and Han, J.-C., 1993: Reynolds number effect on leading edge film effectiveness and heat transfer coefficient. *Int. Journal of Heat and Mass Transfer, Vol.36, 15, pp 3723-3730*

Nirmalan, N.V. and Hylton, L.D., 1990: An Experimental Study of Turbine Vane Heat Transfer with Leading Edge and Downstream Film Cooling. *Journal of Turbomachinery, Vol.112, July 1990, pp 477-487*

Reiss, H. and Bölcs, A., 2000: Experimental Study of Showerhead Cooling on a Cylinder Comparing Several Configurations using Cylindrical and Shaped Holes. *Journal of Turbomachinery, Vol.122, Jan. 2000*

Reiss, H., Bölcs, A. and Drost, U., 1998: The Transient Liquid Crystal Technique Employed for Sub- and Transonic Heat Transfer and Film Cooling Measurements in a Linear Cascade. *U. o. Limerick, XIV biennial Symposium on Measuring Techniques in Transonic and Supersonic Flow in Cascades and Turbomachinery, Limerick, Ireland*

Vedula, R.J. and Metzger, D.E., 1991: A method for the simultaneous determination of local effectiveness and heat transfer distributions in three-temperature convection situations. *ASME Paper 91-GT-345 , Orlando, Florida, USA*

Wadia, A.R. and Nealy, D.A., 1985: Development of a design model for airfoil leading edge film cooling. *ASME Paper 85-GT-120*